MATERIALS SCIENCE

10.1126/sciadv.1500222

Ultrahigh-mobility graphene devices from chemical vapor deposition on reusable copper

Luca Banszerus,[1]* Michael Schmitz,[1]* Stephan Engels,[1,2]* Jan Dauber,[1,2] Martin Oellers,[1] Federica Haupt,[3] Kenji Watanabe,[4] Takashi Taniguchi,[4] Bernd Beschoten,[1] Christoph Stampfer[1,2]†

Graphene research has prospered impressively in the past few years, and promising applications such as high-frequency transistors, magnetic field sensors, and flexible optoelectronics are just waiting for a scalable and cost-efficient fabrication technology to produce high-mobility graphene. Although significant progress has been made in chemical vapor deposition (CVD) and epitaxial growth of graphene, the carrier mobility obtained with these techniques is still significantly lower than what is achieved using exfoliated graphene. We show that the quality of CVD-grown graphene depends critically on the used transfer process, and we report on an advanced transfer technique that allows both reusing the copper substrate of the CVD growth and making devices with mobilities as high as 350,000 $cm^2 V^{-1} s^{-1}$, thus rivaling exfoliated graphene.

INTRODUCTION

Chemical vapor deposition (CVD) on copper (*1*–*11*) is a convenient alternative to epitaxial growth (*12*–*16*) for obtaining large graphene crystals. However, to serve as channel material in electronic devices such as high-frequency transistors (*17*), Hall sensors (*18*), and various other applications (*19*), CVD-grown graphene needs to be transferred from the growth substrate (typically copper) onto an insulating substrate, for example, SiO_2 or hexagonal boron nitride (hBN). In state-of-the-art transfer methods (*20*), a transfer polymer is deposited directly onto the graphene, and the copper substrate is chemically etched away. This approach has two major drawbacks: first, chemical residues strongly degrade the electronic properties of graphene and reduce its mobility well below the values obtained in exfoliated graphene; second, it leaves no copper to be reused in a new growth step and thereby significantly increases the production costs and creates chemical waste. An alternative, very promising transfer method is delamination. In this case, graphene is peeled from the growth surface by exerting an external force, thus preserving the copper foil for reuse. Both electrochemical (*21*, *22*) and dry delamination (*23*) of CVD-grown graphene have been recently demonstrated. However, the electronic quality of the graphene obtained in these pioneering works still appears to suffer from chemical- and process-related contaminations.

Here, we report on a delamination method that overcomes these problems and results in CVD-grown graphene devices with properties comparable to those of high-quality exfoliated graphene. The key aspect is an advanced transfer process based on van der Waals forces, which we use to pick up CVD-grown graphene directly from the copper and to encapsulate it in hBN while avoiding any contact with intermediary epoxy, polymers, or other chemical agents. This method minimizes all contaminations of the graphene surface due to processing and, at the same time, allows performance of multiple growth cycles on the same copper substrate. The high quality of the hBN/graphene heterostructures obtained using this method is probed by Raman spectroscopy and transport measurements. All investigated devices exhibit an extremely narrow Raman 2D peak and high carrier mobilities ($\mu \approx 100{,}000$ $cm^2 V^{-1} s^{-1}$ or higher), similar to those observed in hBN/graphene heterostructure based on exfoliated graphene (*24*, *25*). Remarkably, we observe no noticeable difference between devices realized in the first or subsequent growth cycles, indicating that the copper substrate is a reusable resource in our fabrication process.

RESULTS

Graphene flakes are grown by low-pressure CVD (*1*, *10*, *26*), using methane as a precursor and copper as a growth substrate (see Materials and Methods). A schematic of the furnace is illustrated in Fig. 1A, whereas Fig. 1G shows a scanning electron microscopy (SEM) image of a typical graphene flake on copper. The diameter of the flakes can reach up to hundreds of micrometers (*1*, *10*) (see also the Supplementary Materials). After a few days of exposure to ambient conditions, the graphene flakes on copper undergo a significant change in optical contrast and become visible with an optical microscope (see Fig. 1C). Energy-dispersive x-ray (EDX) spectroscopy indicates that this change of contrast is associated with an increased concentration of oxygen at the graphene-copper interface (see the Supplementary Materials), which is in agreement with the recent observations by Schriver *et al.* (*27*), that CVD graphene actually promotes the oxidation of copper at room temperature. Although this effect might be detrimental for certain applications, it increases the success rate of the dry delamination method illustrated in Fig. 1B to above 90%, without affecting the electronic properties of the transferred graphene. Details on the transfer process are given in Materials and Methods. In brief, we prepare a polymer stack consisting of polyvinylalcohol (PVA) and polymethylmethacrylate (PMMA) on a polydimethylsiloxane (PDMS) stamp. The stack is covered with an exfoliated hBN flake and brought into contact with the graphene on copper. Thanks to the strong van der Waals interactions between the graphene and the hBN, the graphene is picked up from its growth substrate when separating the stack again. It can then be transferred to an arbitrary substrate, for example, another exfoliated hBN flake, as for the samples investigated in this work.

This transfer process allows reuse of the catalyst foil in multiple growth cycles. This is exemplified in Fig. 1, D and E, where we show graphene grown on the very same copper substrate in two subsequent

[1]JARA-FIT and 2nd Institute of Physics, RWTH Aachen University, 52074 Aachen, Germany. [2]Peter Grünberg Institute (PGI-9), Forschungszentrum Jülich, 52425 Jülich, Germany. [3]JARA–Institute for Quantum Information, RWTH Aachen University, 52056 Aachen, Germany. [4]National Institute for Materials Science, 1-1 Namiki, Tsukuba 305–0044, Japan.
*These authors contributed equally to this work.
†Corresponding author. E-mail: stampfer@physik.rwth-aachen.de

growth cycles, that is, the flakes in Fig. 1E were grown after those in Fig. 1D were picked up with the transfer technique described above. The arrow indicates a marker cut that was manually placed on copper after the first growth process, to unambiguously identify the specific location on the substrate. The flakes obtained in both growth cycles are similar in size and shape and, as we show below, in structural and electronic properties.

The properties of the CVD graphene/hBN heterostructures are probed by Raman and electrical transport measurements. A typical Raman spectrum is shown in Fig. 2A. It is comparable to the spectra obtained for exfoliated graphene sandwiched in hBN (*25*, *28*–*31*). The graphene-related G and 2D peaks are visible at positions ω_G = 1584.2 cm^{-1} and ω_{2D} = 2687.2 cm^{-1}. The absence of the D peak around $\omega_D \approx 1345$ cm^{-1} indicates the lack of lattice defects (*32*), giving a first evidence of the high structural quality of the fabricated heterostructure. A second and equally important clue comes from the exceptionally small full width at half maximum (FWHM) of the 2D peak, $\Gamma_{2D} \approx 16.5$ cm^{-1}. It has recently been shown that random strain variations on the nanometer scale are the main source of broadening of the Raman 2D peak and that low values of Γ_{2D} are a direct indication of a uniform strain landscape within the laser spot size (*25*).

For all samples, we record spatially resolved Raman maps as shown in Fig. 2B, and plot the values of Γ_{2D} in histograms, such as in Fig. 2C. From these, we extract the sample-averaged width of the 2D peak, $\overline{\Gamma_{2D}}$. For comparison, we also repeat the same procedure on a number of samples with CVD-grown graphene wet-transferred to SiO_2 or sandwiched between hBN flakes using the state-of-the-art wet etching technique (*20*). The obtained Γ_{2D} values for the wet-transferred samples are in agreement with literature (*33*). Remarkably, all heterostructures produced with the dry delamination method show a value of $\overline{\Gamma_{2D}}$ about 20 cm^{-1}, significantly smaller than what is observed in wet-transferred

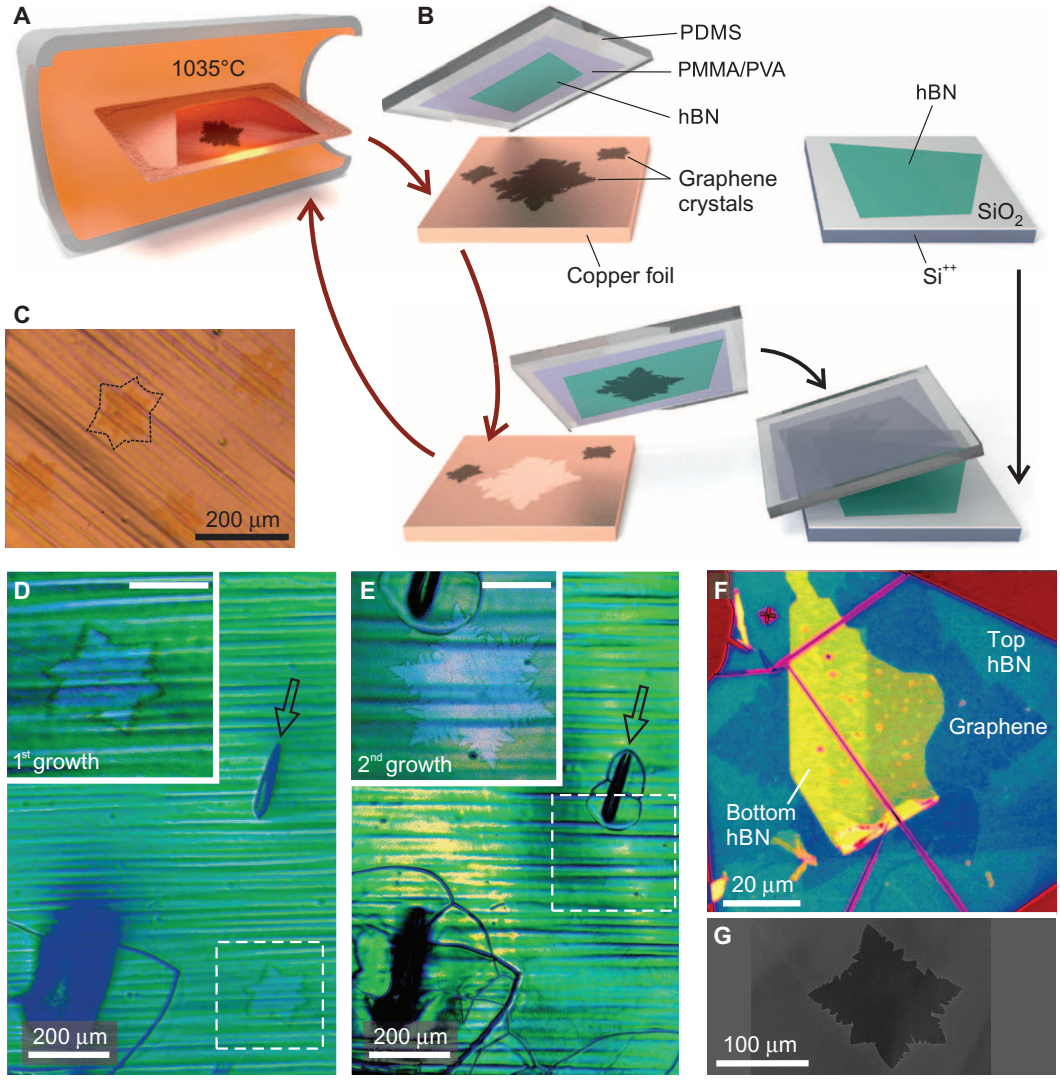

Fig. 1. Dry transfer of CVD-grown graphene. (**A**) Illustration of the CVD furnace with a copper enclosure inside. (**B**) Process schematic of the contamination-free transfer of CVD graphene from copper onto hBN. (**C**) Optical microscopy image of grown graphene crystals on copper foil. (**D** and **E**) Optical false-color image of graphene on copper after a first (D) and a second (E) growth cycle. The insets show close-ups of areas marked by the dashed rectangles (see also fig. S1). (**F**) False-color optical image of CVD graphene encapsulated in hBN. The graphene is recognizable by its fractal shape. Turquoise and yellow areas correspond to the top and bottom hBN flakes, respectively (see also fig. S2). (**G**) SEM image of a graphene crystal on copper.

samples (see Fig. 2D). This also holds true for the average strain in the samples, which we estimate following (*34*) by analyzing ω_G and ω_{2D} (see the Supplementary Materials). The clustering of the diamond-shaped data points in Fig. 2D further shows that our fabrication technique consistently results in samples of high structural quality, with low strain values (about 0.1%) and small strain fluctuations on the nanometer scale over the entire sample, manifested by low values of $\overline{\Gamma_{2D}}$ (*25*). Moreover, structures fabricated by reusing the copper substrate multiple times show the same properties as those realized in the first growth cycle (see Fig. 2, D and E).

Random strain variations not only affect the linewidth of the Raman 2D peak but also are the dominant cause of scattering for electrons in graphene on hBN (*31*). Being characterized by remarkably low values of $\overline{\Gamma_{2D}}$, our samples hold promise to show high carrier mobility. We test this by performing transport measurements in a four-probe configuration, after structuring the CVD graphene/hBN heterostructures into Hall bar devices and contacting them following the scheme of Wang *et al.* (*24*). An optical image of a typical device is shown in the inset of Fig. 3A, together with the four-terminal resistance measured as a function of back-gate voltage V_{BG} at low (T = 1.6 K, blue) and at room temperature (T = 300 K, black curve). The small shift of the peaks with respect to V_{BG} = 0 V represents a doping level of 3×10^{11} cm^{-2}. The mobility of each sample is extracted by plotting the conductivity as a function of the charge carrier density n (Fig. 3B), performing a linear regression up to $n = 5 \times 10^{11}$ cm^{-2}, and calculating the mobility in terms of the Drude formula (see also the Supplementary Materials). For the sample shown in Fig. 3A at T = 1.6 K, we obtain μ = 110,000 and 145,000 cm^2 V^{-1} s^{-1} for electrons and holes, respectively. The green curve in Fig. 3B represents the low temperature conductivity of another sample with carrier mobilities of μ = 320,000 and 350,000 cm^2 V^{-1} s^{-1} for electrons and holes, respectively. These values exceed the highest ones reported for CVD graphene (*6*, *9*) by roughly one order of magnitude and, when performing magnetotransport measurements, are reflected in a very well resolved Landau fan and broken Landau level degeneracy already at moderately low magnetic fields (see Fig. 3C and fig. S3). Similar features have previously been observed in high-quality devices based on exfoliated graphene

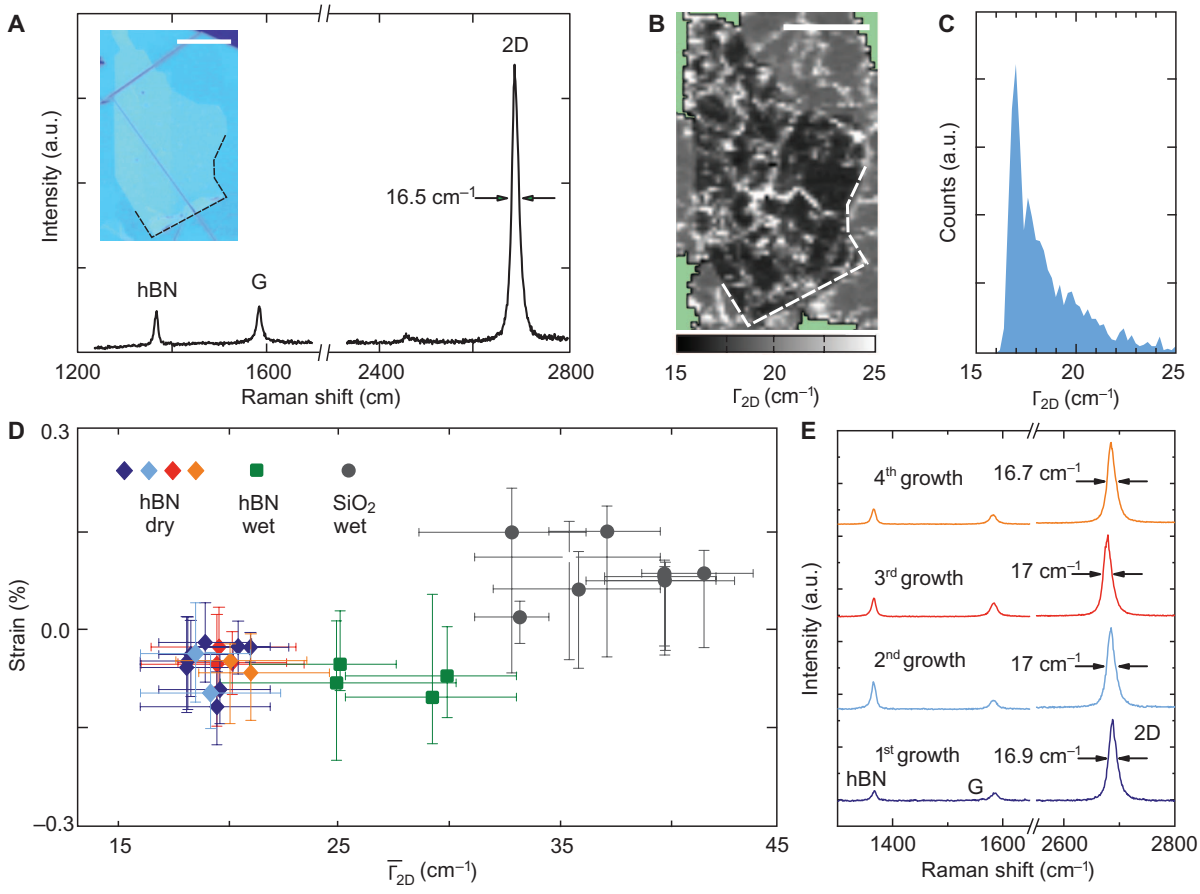

Fig. 2. Raman characterization of CVD-grown graphene. (**A**) Typical Raman spectrum and microscopy image (inset) of a CVD graphene/hBN heterostructure. a.u., arbitrary units. (**B**) Spatially resolved map of the width of the 2D peak, Γ_{2D}, measured in the region displayed in (A). Scale bars, 20 μm. Γ_{2D} shows remarkably low values in the area where the graphene flake is encapsulated in hBN [marked by the dashed line, see also inset in (A)]. (**C**) Histogram of Γ_{2D} measured on the encapsulated part of the graphene flake shown in (B). It exhibits a maximum at 16.8 cm^{-1} and a cutoff at 16 cm^{-1}. (**D**) Sample-averaged $\overline{\Gamma_{2D}}$ against average strain for 29 samples. Squared and circle data points correspond to CVD-grown graphene wet-transferred to SiO_2 and between hBNs, respectively. Diamond-shaped data points correspond to samples realized with the dry transfer technique starting from a new or a reused copper substrate. Different colors correspond to different growth cycles, according to the color scheme of (E). For each data point, the error bars indicate the 20th and 80th percentile of the corresponding distributions of Γ_{2D} and strain. (**E**) Typical Raman spectra of samples made with the dry transfer technique performing multiple growth cycles on the same copper substrate.

(*35*). At higher temperatures, the mobility of our samples shows the expected tendency to decrease, but remains well above 50,000 $cm^2 V^{-1} s^{-1}$ up to room temperature (see Fig. 3F), making our fabrication method very appealing for technological applications.

Another indication of the sample quality is given by the disorder-induced charge carrier density fluctuations n^*. This quantity gives a measure of the potential fluctuations experienced by the electrons (*31*). It can be extracted by plotting the low-temperature conductivity σ against the carrier density n in a double logarithmic scale (see Fig. 3E). For all our devices, we extract very low values of n^*, around a few 10^{10} cm^{-2}, which indicate a rather homogeneous potential background. Moreover, we again observe no difference between samples fabricated in a first or second growth cycle on the same copper substrate (see blue and red squares in Fig. 4). Comparing these values with those given in literature for devices based on wet-transferred CVD graphene (see circles in Fig. 4) (*6*), we can conclude that our fabrication technique leads consistently to devices with higher mobility and smaller potential fluctuations than those that can be achieved with the wet-transfer method.

DISCUSSION

In summary, we demonstrated that it is possible to use the van der Waals interaction between hBN and graphene to pick up CVD-grown graphene flakes from their growth substrate and to deposit them on an arbitrary substrate. This allows the polymer-free assembly of hBN/CVD-grown graphene heterostructures with electronic properties comparable to those reported for similar devices based on exfoliated graphene (*24*). This proves that CVD-grown graphene is not inferior to ultrahigh-mobility exfoliated graphene, if transferred appropriately.

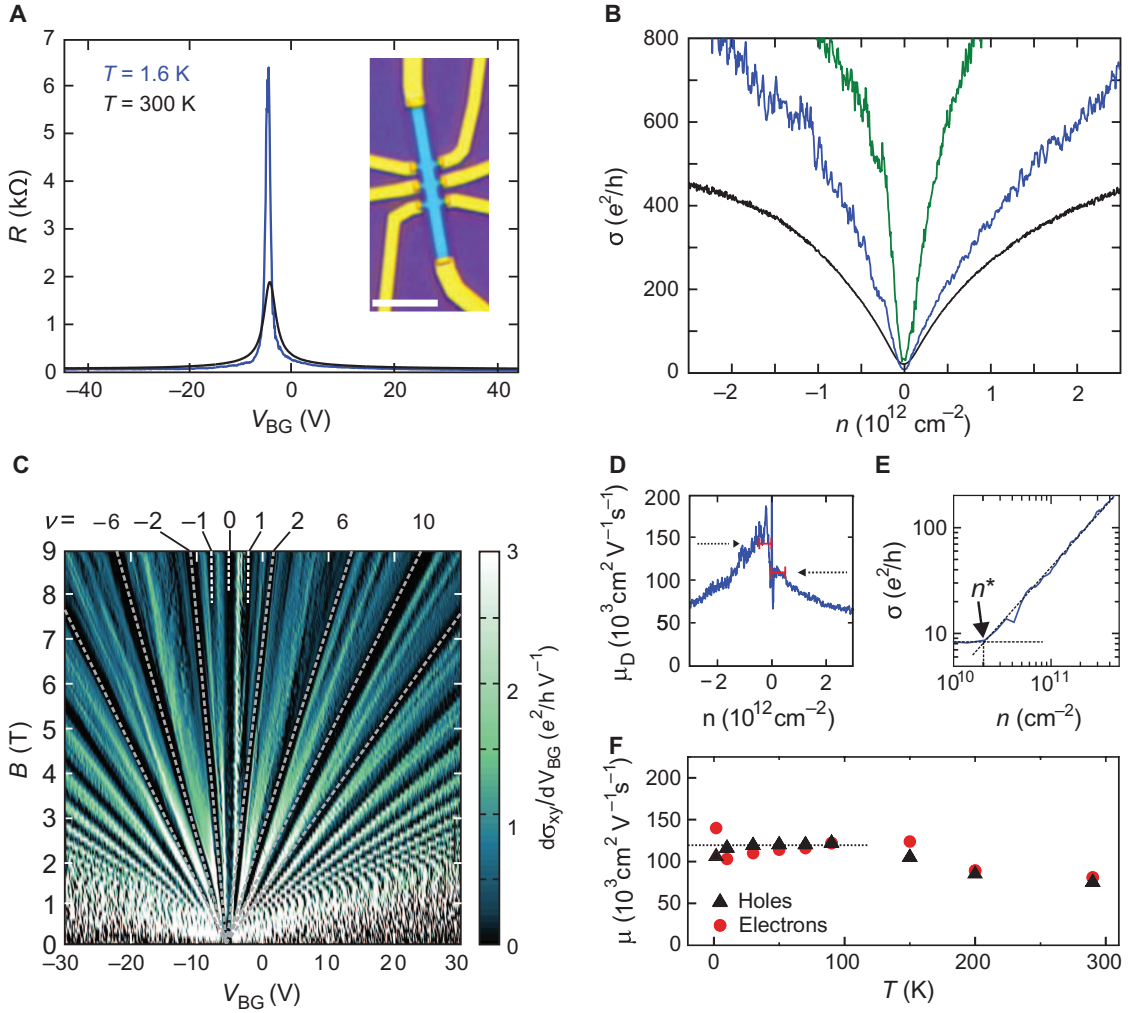

Fig. 3. Transport characterization of dry-assembled devices. (**A**) Optical image of a Hall bar device and four-terminal resistance as a function of back-gate voltage at 1.6 K (blue) and 300 K (black). (**B**) Conductance σ as a function of charge carrier density n for the device shown in (A). The green curve shows data measured on another sample with carrier mobility of μ = 350,000 $cm^2 V^{-1} s^{-1}$. (**C**) Derivative of the Hall conductivity σ_{xy} with respect to V_{BG} as a function of magnetic field B and V_{BG} for the device corresponding to the green curve in (B). Landau levels (LL) at filling factors $\nu = \ldots, -10, -6, -2, 0, 2, 6, 10, \ldots$ are clearly visible. Several LL exhibit full degeneracy lifting already at $B = 6$ T, see, for example, the appearance of LL at $\nu = -1, 1$. (**D**) Plot of $\mu_D = \sigma/ne$ as a function of the charge carrier density for the device shown in (A) at 1.6 K. The dashed lines represent the mobilities extracted from (B). (**E**) Procedure to extract n^*: two lines are fitted to the double logarithmic plot of σ as a function of n. (**F**) Mobility as a function of temperature for the device shown in (A).

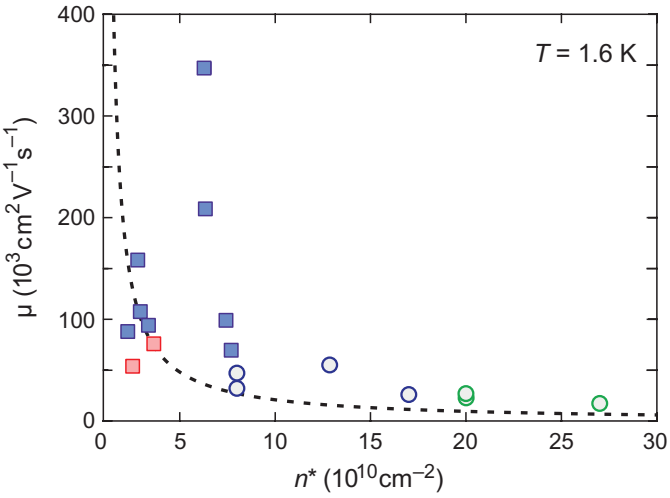

Fig. 4. Mobility and disorder-induced charge carrier fluctuations *n of CVD-grown graphene samples.** Disorder-induced charge carrier density fluctuation *n** and charge carrier mobility μ (averaged over both carrier types) for 10 Hall bar devices fabricated from graphene encapsulated in hBN, using the dry transfer technique (rectangles). The red data points correspond to samples from reused copper. Circle data points correspond to the transport data reported by Petrone *et al.* (*6*) for Hall bars on hBN (blue) and SiO_2 (green) (*39*). The dashed line represents the inverse relation between the two quantities plotted and is taken from (*31*).

Moreover, it demonstrates once more that it is mandatory to protect the graphene surface from processing-related contaminations to obtain high-performance graphene devices. Indeed, the critical feature of our transfer method compared with previous delamination techniques (*21*–*23*) is that throughout the fabrication process graphene gets into contact only with hBN, which is an ideal dielectric for high-performance graphene devices (*35*). Currently, the size of the hBN flakes poses an ultimate limit to the dimensions of our samples. However, this limitation might be circumvented by current progresses in the CVD synthesis of large hBN flakes (*36*), thus leading the way toward a scalable technology for high-quality graphene devices.

MATERIALS AND METHODS

CVD growth of large graphene crystals

The graphene flakes were grown by CVD on commercially available copper foil (Alfa Aesar no. 46365). Before growth, the copper is etched in a 0.05 M solution of ammonium persulfate for 2 min to clean the surface. Afterward, it is rinsed in deionized water, in acetone, and in isopropyl alcohol and dried in a stream of nitrogen. A tight enclosure is then folded from the foil to prevent evaporative losses of copper during growth (*10*). The growth is carried out in a quartz tube with an inner diameter of 8 cm, following the scheme shown in fig. S4A: the temperature is ramped to 1035°C under a 10-sccm flow of hydrogen, resulting in a pressure of 7×10^{-3} mbar. The enclosure is then annealed under these conditions for 20 min. The graphene growth is initiated by increasing the hydrogen flow to 45 sccm and introducing a 1.3-sccm flow of methane into the system. After a growth time of 2 hours, the sample is rapidly cooled down to room temperature. Figure S4B shows a dark-field microscopy image (*34*) of a graphene crystal grown on the inside of the enclosure, with a diameter larger than 500 μm. Investigations by SEM reveal that the crystals are free of adlayers and other irregularities (fig. S4, C and D).

Contamination-free dry transfer method

We prepared a two-layered transfer polymer composed of layers of PVA and PMMA on a coated glass slide to obtain a flat polymer foil. We then exfoliated hBN on the polymer and searched for a flat and clean hBN flake using optical microscopy. We cut out the piece of polymer supporting the flake, removed it from the glass slide, and placed it on a thin slice of PDMS. With this procedure, we obtained a stack of PDMS/PVA/PMMA/hBN. This stack is brought into mechanical contact with the graphene on copper (hBN down) at a temperature of $T = 125$°C and separated thereafter. When lifting the stack, graphene is picked up from the copper thanks to the strong van der Waals interaction between graphene and hBN. The hBN/polymer stack with the graphene residing on top is then deposited on a second hBN flake that has been previously exfoliated on Si/SiO_2. Because the PDMS is only loosely attached to the PVA, it can easily be removed. Afterward, we dissolved the PVA with water and PMMA with acetone. With this method, we obtained an hBN/graphene/hBN heterostructure on Si/SiO_2. Atomic force microscopy investigations of the heterostructures indicate the existence of small bubbles (see fig. S5B), as observed also on similar samples fabricated from exfoliated graphene (*30*). To structure the Hall bars, a hard mask is patterned using e-beam lithography. Then, the sample is etched using reactive ion etching with SF_6 and Ar. After removing the hard mask, contacts consisting of 5 nm chromium and 90 nm gold are evaporated onto the samples.

SUPPLEMENTARY MATERIALS

Supplementary material for this article is available at http://advances.sciencemag.org/cgi/content/full/1/6/e1500222/DC1

Text

Fig. S1. Original data corresponding to Fig. 1 (D and E).

Fig. S2. Original data corresponding to Fig. 1F.

Fig. S3. Magnetotransport measurements.

Fig. S4. Wet-transferred graphene flakes.

Fig. S5. Dry-assembled hBN/graphene/hBN heterostructures.

Fig. S6. CVD growth of large graphene flakes.

Fig. S7. EDX analysis of a graphene flake on copper.

Fig. S8. EDX line scans for the oxygen K-line on three different samples.

Fig. S9. Analysis of the strain in dry-assembled hBN/graphene/hBN heterostructure.

Fig. S10. Linear versus Boltzmann fit of the conductance.

Fig. S11. Carrier density–dependent mobility μ_D for six different samples.

References (*37*, *38*)

REFERENCES AND NOTES

1. X. Li, W. Cai, J. An, S. Kim, J. Nah, D. Yang, R. Piner, A. Velamakanni, I. Jung, E. Tutuc, S. K. Banerjee, L. Colombo, R. S. Ruoff, Large-area synthesis of high-quality and uniform graphene films on copper foils. *Science* **324**, 1312–1314 (2009).
2. S. Bae, H. Kim, Y. Lee, X. Xu, J. S. Park, Y. Zheng, J. Balakrishnan, T. Lei, H. R. Kim, Y. I. Song, Y. J. Kim, K. S. Kim, B. Ozyilmaz, J. H. Ahn, B. H. Hong, S. Iijima, Roll-to-roll production of 30-inch graphene films for transparent electrodes. *Nat. Nanotechnol.* **5**, 574–578 (2010).
3. S. Bhaviripudi, X. Jia, M. S. Dresselhaus, J. Kong, Role of kinetic factors in chemical vapor deposition synthesis of uniform large area graphene using copper catalyst. *Nano Lett.* **10**, 4128–4133 (2010).
4. L. Gan, Z. Luo, Turning off hydrogen to realize seeded growth of subcentimeter single-crystal graphene grains on copper. *ACS Nano* **7**, 9480–9488 (2013).
5. Y. Hao, M. S. Bharathi, L. Wang, Y. Liu, H. Chen, S. Nie, X. Wang, H. Chou, C. Tan, B. Fallahazad, H. Ramanarayan, C. W. Magnuson, E. Tutuc, B. I. Yakobson, K. F. McCarty, Y. W. Zhang, P. Kim,

J. Hone, L. Colombo, R. S. Ruoff, The role of surface oxygen in the growth of large single-crystal graphene on copper. *Science* **342**, 720–723 (2013).
6. N. Petrone, C. R. Dean, I. Meric, A. M. van der Zande, P. Y. Huang, L. Wang, D. Muller, K. L. Shepard, J. Hone, Chemical vapor deposition-derived graphene with electrical performance of exfoliated graphene. *Nano Lett.* **12**, 2751–2756 (2012).
7. I. Vlassiouk, M. Regmi, P. Fulvio, S. Dai, P. Datskos, G. Eres, S. Smirnov, Role of hydrogen in chemical vapor deposition growth of large single-crystal graphene. *ACS Nano* **5**, 6069–6076 (2011).
8. Z. Yan, J. Lin, Z. Peng, Z. Sun, Y. Zhu, L. Li, C. Xiang, E. L. Samuel, C. Kittrell, J. M. Tour, Toward the synthesis of wafer-scale single-crystal graphene on copper foils. *ACS Nano* **6**, 9110–9117 (2012).
9. V. E. Calado, S.-E. Zhu, S. Goswami, Q. Xu, K. Watanabe, T. Taniguchi, G. C. A. M. Janssen, L. M. K. Vandersypen, Ballistic transport in graphene grown by chemical vapor deposition. *Appl. Phys. Lett.* **104**, 023103 (2014).
10. S. Chen, H. Ji, H. Chou, Q. Li, H. Li, J. W. Suk, R. Piner, L. Liao, W. Cai, R. S. Ruoff, Millimeter-size single-crystal graphene by suppressing evaporative loss of Cu during low pressure chemical vapor deposition. *Adv. Mater.* **25**, 2062–2065 (2013).
11. A. W. Tsen, L. Brown, M. P. Levendorf, F. Ghahari, P. Y. Huang, R. W. Havener, C. S. Ruiz-Vargas, D. A. Muller, P. Kim, J. Park, Tailoring electrical transport across grain boundaries in polycrystalline graphene. *Science* **336**, 1143–1146 (2012).
12. K. V. Emtsev, A. Bostwick, K. Horn, J. Jobst, G. L. Kellogg, L. Ley, J. L. McChesney, T. Ohta, S. A. Reshanov, J. Röhrl, E. Rotenberg, A. K. Schmid, D. Waldmann, H. B. Weber, T. Seyller, Towards wafer-size graphene layers by atmospheric pressure graphitization of silicon carbide. *Nat. Mater.* **8**, 203–207 (2009).
13. C. Berger, Z. Song, X. Li, X. Wu, N. Brown, C. Naud, D. Mayou, T. Li, J. Hass, A. N. Marchenkov, E. H. Conrad, P. N. First, W. A. de Heer, Electronic confinement and coherence in patterned epitaxial graphene. *Science* **312**, 1191–1196 (2006).
14. P. W. Sutter, J.-I. Flege, E. A. Sutter, Epitaxial graphene on ruthenium. *Nat. Mater.* **7**, 406–411 (2008).
15. J. H. Lee, E. K. Lee, W. J. Joo, Y. Jang, B. S. Kim, J. Y. Lim, S. H. Choi, S. J. Ahn, J. R. Ahn, M. H. Park, C. W. Yang, B. L. Choi, S. W. Hwang, D. Whang, Wafer-scale growth of single-crystal monolayer graphene on reusable hydrogen-terminated germanium. *Science* **344**, 286–289 (2014).
16. Z. R. Robinson, P. Tyagi, T. R. Mowll, C. A. Ventrice Jr., J. B. Hannon, Argon-assisted growth of epitaxial graphene on Cu(111). *Phys. Rev. B* **86**, 235413 (2012).
17. Y. M. Lin, C. Dimitrakopoulos, K. A. Jenkins, D. B. Farmer, H. Y. Chiu, A. Grill, P. Avouris, 100-GHz transistors from wafer-scale epitaxial graphene. *Science* **327**, 662 (2010).
18. L. Huang, H. Xu, Z. Zhang, C. Chen, J. Jiang, X. Ma, B. Chen, Z. Li, H. Zhong, L.-M. Peng, Graphene/Si CMOS hybrid Hall integrated circuits. *Sci. Rep.* **4**, 5548 (2014).
19. K. S. Novoselov, V. I. Fal'ko, L. Colombo, P. R. Gellert, M. G. Schwab, K. Kim, A roadmap for graphene. *Nature* **490**, 192–200 (2012).
20. J. W. Suk, A. Kitt, C. W. Magnuson, Y. Hao, S. Ahmed, J. An, A. K. Swan, B. B. Goldberg, R. S. Ruoff, Transfer of CVD-grown monolayer graphene onto arbitrary substrates. *ACS Nano* **5**, 6916–6924 (2011).
21. Y. Wang, Y. Zheng, X. Xu, E. Dubuisson, Q. Bao, J. Lu, K. P. Loh, Electrochemical delamination of CVD-grown graphene film: Toward the recyclable use of copper catalyst. *ACS Nano* **5**, 9927–9933 (2011).
22. X. Wang, L. Tao, Y. Hao, Z. Liu, H. Chou, I. Kholmanov, S. Chen, C. Tan, N. Jayant, Q. Yu, D. Akinwande, R. S. Ruoff, Direct delamination of graphene for high-performance plastic electronics. *Small* **10**, 694–698 (2014).
23. T. Yoon, W. C. Shin, T. Y. Kim, J. H. Mun, T. S. Kim, B. J. Cho, Direct measurement of adhesion energy of monolayer graphene as-grown on copper and its application to renewable transfer process. *Nano Lett.* **12**, 1448–1452 (2012).
24. L. Wang, I. Meric, P. Y. Huang, Q. Gao, Y. Gao, H. Tran, T. Taniguchi, K. Watanabe, L. M. Campos, D. A. Muller, J. Guo, P. Kim, J. Hone, K. L. Shepard, C. R. Dean, One-dimensional electrical contact to a two-dimensional material. *Science* **342**, 614–617 (2013).
25. C. Neumann, S. Reichardt, P. Venezuela, M. Drögeler, L. Banszerus, M. Schmitz, K. Watanabe, T. Taniguchi, F. Mauri, B. Beschoten, S. V. Rotkin, C. Stampfer, Raman spectroscopy as probe of nanometer-scale strain variations in graphene. arXiv:1406.7771v2 (2015).
26. X. Li, C. W. Magnuson, A. Venugopal, R. M. Tromp, J. B. Hannon, E. M. Vogel, L. Colombo, R. S. Ruoff, Large-area graphene single crystals grown by low-pressure chemical vapor deposition of methane on copper. *J. Am. Chem. Soc.* **133**, 2816–2819 (2011).
27. M. Schriver, W. Regan, W. J. Gannett, A. M. Zaniewski, M. F. Crommie, A. Zettl, Graphene as a long-term metal oxidation barrier: Worse than nothing. *ACS Nano* **7**, 5763–5768 (2013).
28. A. C. Ferrari, J. C. Meyer, V. Scardaci, C. Casiraghi, M. Lazzeri, F. Mauri, S. Piscanec, D. Jiang, K. S. Novoselov, S. Roth, A. K. Geim, Raman spectrum of graphene and graphene layers. *Phys. Rev. Lett.* **97**, 187401 (2006).
29. D. Graf, F. Molitor, K. Ensslin, C. Stampfer, A. Jungen, C. Hierold, L. Wirtz, Spatially resolved Raman spectroscopy of single- and few-layer graphene. *Nano Lett.* **7**, 238–242 (2007).
30. F. Forster, A. Molina-Sanchez, S. Engels, A. Epping, K. Watanabe, T. Taniguchi, L. Wirtz, C. Stampfer, Dielectric screening of the Kohn anomaly of graphene on hexagonal boron nitride. *Phys. Rev. B* **88**, 085419 (2013).
31. N. J. G. Couto, D. Costanzo, S. Engels, D.-K. Ki, K. Watanabe, T. Taniguchi, C. Stampfer, F. Guinea, A. F. Morpurgo, Random strain fluctuations as dominant disorder source for high-quality on-substrate graphene devices. *Phys. Rev. X* **4**, 041019 (2014).
32. A. C. Ferrari, D. M. Basko, Raman spectroscopy as a versatile tool for studying the properties of graphene. *Nat. Nanotechnol.* **8**, 235–246 (2013).
33. K. Chattrakun, S. Huang, K. Watanabe, T. Taniguchi, A. Sandhu, B. J. LeRoy, Gate dependent Raman spectroscopy of graphene on hexagonal boron nitride. *J. Phys. Condens. Matter* **25**, 505304 (2013).
34. J. E. Lee, G. Ahn, J. Shim, Y. S. Lee, S. Ryu, Optical separation of mechanical strain from charge doping in graphene. *Nat. Commun.* **3**, 1024 (2012).
35. C. R. Dean, A. F. Young, I. Meric, C. Lee, L. Wang, S. Sorgenfrei, K. Watanabe, T. Taniguchi, P. Kim, K. L. Shepard, J. Hone, Boron nitride substrates for high-quality graphene electronics. *Nat. Nanotechnol.* **5**, 722–726 (2010).
36. S. Caneva, R. S. Weatherup, B. C. Bayer, B. Brennan, S. J. Spencer, K. Mingard, A. Cabrero-Vilatela, C. Baehtz, A. J. Pollard, S. Hofmann, Nucleation control for large, single crystalline domains of monolayer hexagonal boron nitride via Si-doped Fe catalysts. *Nano Lett.* **15**, 1867–1875 (2015).
37. X. Kong, H. X. Ji, R. D. Piner, H. F. Li, C. W. Magnuson, C. Tan, A. Ismach, H. Chou, R. S. Ruoff, Non-destructive and rapid evaluation of chemical vapor deposition graphene by dark field optical microscopy. *Appl. Phys. Lett.* **103**, 043119 (2013).
38. K. Nomura, A. H. MacDonald, Quantum transport of massless Dirac fermions. *Phys. Rev. Lett.* **98**, 076602 (2007).
39. The Supplementary Information of Petrone et al. (*6*) contains a table with transport data for several CVD-grown graphene devices on SiO_2 and hBN. The values for the mobility given there were extracted using the same method used for our samples, and were obtained at the same temperature. For each sample, the disorder-induced charge carrier fluctuations n^* can be estimated from the FWHM of the Dirac peak, ΔW_{CNP}, following Dean *et al*. (*35*).

Acknowledgments: We thank S. Reichardt for helpful discussions and M. Goldsche for evaporating the metal contacts. **Funding:** Support by the Helmholtz Nanoelectronic Facility (HNF), the Deutsche Forschungsgemeinschaft (DFG) (SPP-1459), the ERC (GA-Nr. 280140), and the EU project Graphene Flagship (contract no. NECT-ICT-604391) is gratefully acknowledged. **Author contributions:** L.B., M.S., S.E., F.H., B.B., and C.S. conceived the experiment and analyzed the data. L.B., M.S., S.E., J.D., and M.O. fabricated the samples. L.B., M.S., and S.E. made the measurements. L.B., F.H., M.S., S.E., B.B., and C.S. wrote the paper. T.T. and K.W. synthesized the hBN crystals. B.B. and C.S. advised on experiments. **Competing interests:** The authors declare that they have no competing interests.

Submitted 3 March 2015
Accepted 31 May 2015
Published 31 July 2015
10.1126/sciadv.1500222

Citation: L. Banszerus, M. Schmitz, S. Engels, J. Dauber, M. Oellers, F. Haupt, K. Watanabe, T. Taniguchi, B. Beschoten, C. Stampfer, Ultrahigh-mobility graphene devices from chemical vapor deposition on reusable copper. *Sci. Adv.* **1**, e1500222 (2015).